REPORT DOCUMENTATION PAGE

AFRL-SR-BL-TR-98-

0257

1. AGENCY USE ONLY (Leave blank)	2. REPORT DATE	3. REPORT TYPE AND DATES COVERED
	2/20/98	FINAL TECH RPT, 01 May 96 to 30 Sep 97

4. TITLE AND SUBTITLE
Participation in the Spring 1996 MISETA HF

5. FUNDING NUMBERS
F49620-96-1-0177

6. AUTHOR(S)
Dr. Michael C. Kelley

7. PERFORMING ORGANIZATION NAME(S) AND ADDRESS(ES)
Cornell University
School of Electrical Engineering
318 Rhodes Hall
Ithaca, NY 14853

8. PERFORMING ORGANIZATION REPORT NUMBER

9. SPONSORING/MONITORING AGENCY NAME(S) AND ADDRESS(ES)
Office of Sponsored Programs
120 Day Hall
Cornell University
Ithaca, NY 14853

nm

10. SPONSORING/MONITORING AGENCY REPORT NUMBER

11. SUPPLEMENTARY NOTES

12a. DISTRIBUTION/AVAILABILITY STATEMENT
Approved for public release; Distribution unlimited.

12b. DISTRIBUTION CODE
Unlimited

13. ABSTRACT *(Maximum 200 words)*

This report summarizes two quite different research tasks conducted under AFOSR Grant F49620-97-1-0177 (Participation in the Spring 1996 MISETA HF Campaign). The transition occurred part way through the program when the Air Force negotiations broke down with Chile. Although we carried out our component of the project in Peru, it became clear that the Air Force Phillips component would not be forthcoming due to diplomatic problems in Chile. At this juncture we began exploring another project of potential interest to the Air Force and describe this briefly in this report as well.

14. SUBJECT TERMS			15. NUMBER OF PAGES
			16. PRICE CODE
17. SECURITY CLASSIFICATION OF REPORT	18. SECURITY CLASSIFICATION OF THIS PAGE	19. SECURITY CLASSIFICATION OF ABSTRACT	20. LIMITATION OF ABSTRACT
unclassified	unclassified	unclassified	UL

NSN 7540-01-280-5500

Standard Form 298 (Rev. 2-89)
Prescribed by ANSI Std 239-18
298-102

Final Technical Report for
AFOSR Grant 96-1-0177

Participation in the Spring 1996 MISETA HF Campaign

Background

This report summarizes two quite different research tasks conducted under AFOSR Grant 96-1-0177 (Participation in the Spring 1996 MISETA HF Campaign). The transition occurred part way through the program when the Air Force negotiations broke down with Chile. Although we carried out our component of the project in Peru, it became clear that the Air Force Phillips component would not be forthcoming due to diplomatic problems in Chile. At this juncture we began exploring another project of potential interest to the Air Force and describe this briefly below as well.

Equatorial Spread F Results

A very detailed report on this project is presented in Appendix A. We carried out some fascinating spread F observations and have found evidence for a new source of free energy, the first such suggestion made in two decades. We anticipate that a refereed publication will be submitted later this year. In carrying out this study we used data from Jicamarca and new analysis techniques from the University of Illinois.

Although the overall goals of the Air Force project were not met, we are confident that our component of the project was carried out well and has produced important new insights on equatorial spread F. Elements will be presented in the opening presentation to be made by the P.I. at the Space Weather Workshop to be held at COMSAT in October.

New Thrust

Late in this period we made contact with Dr. Herb Carlson, acting Chief Scientist at Phillips Laboratory, concerning a proposal to install a modern CCD all-sky imager at the AMOS site on Maui. He was very encouraging and we have detailed plans in place to accomplish this if AFOSR chooses to support the project. An example of a fascinating "wall" of light coursing over the Caribbean is indicated in the figure. Dr. Ed Dewan, of the Air Force Phillips Laboratory, is providing the theoretical basis for the event. The wall may be an atmospheric "bore" analogous to tidal features in the ocean. This event was detected at the same latitude as Hawaii and confirms a prior observation made by a temporary camera on Maui earlier.

We already own the camera and are currently field-testing it in Puerto Rico. We are running the camera through the internet using undergraduate researchers.

The scientific goal is to understand the source of monochromatic waves in the earth's mesosphere. We detect these waves with the airglow variations they produce in three different height zones and hence can learn quite a bit about their character.

A second goal is to provide a climatological basis for the phenomenon in the event that atmospheric science becomes a major player at the AMOS site in the future.

Airglow Image Data from Arecibo, PR
(Jan 6, 1997)

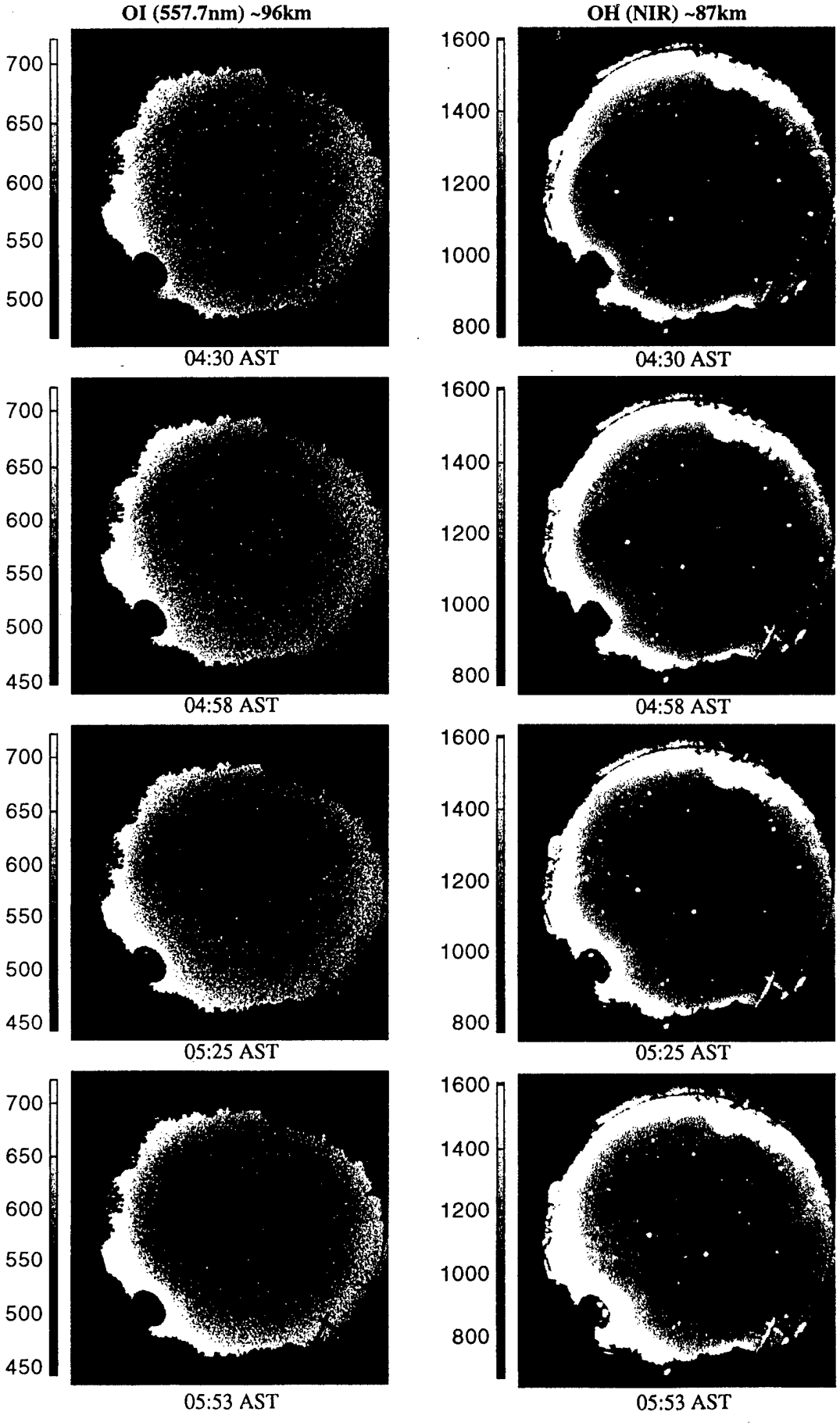

A side benefit is that the Air Force can use our camera to monitor viewing conditions from anywhere in the facility or elsewhere. Although it seems trivial, it is a major effort at times to know if the sky is about to cloud over. Our all-sky camera could prove extremely helpful to operators on site.

This summer a Cornell student spent a week at AMOS and has a detailed plan for installation of the camera, which has been approved in principle by site personnel. Mr. Palmer's report is included in Appendix B.

Publications Related to the Grant

Radar Observations and Numerical Modeling of Bottomside Equatorial Spread F, J.P. Flaherty, Ph.D. thesis, Cornell University, August, 1997.

Simultaneous VHF and transequatorial HF observations in the presence of bottomside equatorial spread F, J.P. Flaherty, M.C. Kelley, C.E. Seyler, and T.J. Fitzgerald, *J. Geophys. Res.*, *101*(A12), 26,811-26,818, 1996.

Technological Transfer

We have developed a user friendly internet instrument interrogation and control interface for an all-sky imager. Already it is being considered for use by the Air Force AMOS operators who need real time information on cloud cover.

Notable Awards and Prizes

Professor Kelley received the Robert '55 and Vanne '57 Cowie Award for Excellence in Teaching from the Cornell College of Engineering in May, 1997.

Appendix A

VHF Measurements on September 17, 1996

VHF Measurements on September 17, 1996

Background

Under the AFOSR grant, we were asked to help plan and support a major Air Force project in Chile by making observations in Peru. We would then provide information on the region at the magnetic equator while Phillip's Laboratory personnel investigated the anomaly zone. Unfortunatley, diplomatic iccues precluded the Chilean component. We carried on, however, and describe the results here.

In this report, we present measurements made at the Jicamarca Radio Observatory during a three hour period on the evening of September 17, 1996. On this evening, irregularities developed on the bottomside of the F layer. For about two hours, the unstable plasma was confined to the bottomside of the layer. After this time, the irregularities began to rise into the dense plasma in the vicinity of the peak of the layer; and eventually, plume-like structures developed and irregularities were observed in the topside of the ionosphere.

Events similar to this have been observed at Jicamarca on numerous occasions. What makes this data set unique is that the measurements were made using a new operating mode for the radar. This new approach to making the measurements was developed by Dr. Ronald Woodman and Professor Erhan Kudeki of the University of Illinois. This new mode greatly improves the quality of the drift measurements made from the incoherent scatter returns. The received signal from the incoherent scatter is weak; in the past, it has usually been necessary to average over all altitudes to produce meaningful calculations of the zonal and vertical drifts. The new mode improves the measurement of the drifts by coherently integrating the component of the incoherent scatter return that is perpendicular to the earth's magnetic

field. The improvement in the measurements makes it no longer necessary to average over all altitudes. For the first time, simultaneous, high-quality measurements of the zonal and vertical velocity as a function of altitude are possible. The new approach to using the radar has already produced many impressive results. One of the most significant results so far is that these measurements have shown the presence of atmospheric gravity wave signatures in the motion of the equatorial F region that have long been hypothesized but not previously measured.

The new procedure for operating the radar makes available much more complete drift information about the background ionosphere than has ever been available in the past. It is also possible to derive information about the structure of the background density from these measurements. Quite importantly for our interest in the role of the shear on the development of the irregularities, this mode, which is described in detail below, also makes it possible to estimate the east-west drift of the irregularities through interferometry. For this data set, the interferometry was effective in determining the zonal drift of the irregularities as a function of altitude and provides a reliable measurement of the shear.

As is well known the vertical and horizontal motion in this region is the result of the electric fields through the $E \times B$ drift. This is an ideal data set for the purpose of studying the role of the vertical and horizontal electric fields on the development of the bottomside irregularities.

Description of the Measurements

The details of the new mode are described in [*Kudeki and Bhattacharyya*, 1997]. The following is a brief discussion of some of the most significant points.

The Jicamarca antenna array contains 9,216 crossed dipole pairs. Each

linear polarization can be steered separately. For these measurements, one polarization is steered to the west and the other is steered to the east. Each of these beams is steered approximately 2.5 deg off of vertical in a direction perpendicular to the Earth's magnetic field, and the angle between the two pointing directions is approximately 5 degrees. On reception, the antenna is divided into two halves. Each of the four receivers are connected to one polarization on one half of the array. The phase centers between the two halves of the antenna are separated by a distance of 24.5 λ, where λ is the free-space wavelength. This forms a single baseline oriented approximately 45 deg with respect to the Earth's magnetic field which can be used with either polarization to do interferometry.

The fundamental observation which motivates the new operating mode is this : for a transmission which is oriented exactly perpendicular to the earth's magnetic field, the correlation time of the incoherent scatter return is extremely long. When a realistic antenna is steered perpendicular to the earth's magnetic field, the autocorrelation of the incoherent scatter returns is finite for a long time [*Woodman and Hagfors*, 1969]. In the past, the radial velocity has been calculated by estimating the change in phase from one pulse to the next. Recognizing that there is information in the signal even at very long lags motivated the question, what is the best way to make use of the complete signal? As is shown in *Kudeki and Bhattacharyya* [1997], the optimal way to process this data is simply to take the Fourier transform of a long time series.

The component of the incoherent scatter return with the long correlation time, of course, has an extremely narrow spectrum. The Doppler of this component can be estimated by simply taking the Fourier transform of a long time series. The Doppler shift of the incoherent scatter is the result of the motion of the background ionosphere in the radial direction. The vertical velocity is calculated by projecting the radial velocity onto the vertical

direction, and the zonal velocity is found by taking the difference between the east and west beams. The assumption in taking the difference between the east and west beams is that the motion in the ionosphere is uniform so that the velocity in both the east and west beams is the same.

Since the received signal from each beam is measured on two antennas which are separated along the east-west direction, it is possible to to use interferometry to make measurements of the position of the scatterer in the east-west plane for each beam. As we will discuss in more detail in subsequent sections, the rate of change of position with time can be used to estimate the velocity of the scatterer.

Interferometry is only possible when there is some correlation between the signals received on the two antennas. Clearly, if there were no correlation between the signals received in the two antennas, then the phase difference between them would have no meaning. For a point source, the signals received by the two antennas are perfectly correlated and the magnitude of the normalized correlation coefficient is unity. If the scattering source has some width, the magnitude of the correlation coefficient will be reduced due to the effects of signals from different directions cancelling each other. If the scattering source is very wide in angle, such as is the case for incoherent scatter, the signals received at the two antennas will be completely decorrelated. For the coherent echoes, which result from irregularities in the plasma, it is possible for the scatterers to be sufficiently localized so that the signals received on the two antennas are highly correlated. For these signals, interferometric techniques can be applied.

As will be described in more detail in the following sections, the processing begins with taking the Fourier transform of the signal, and interferometry is performed in each Doppler cell. The main limitation of this technique is that there is only a single interferometric baseline. If there are multiple sources in the scattering volume that cannot be separated through Doppler processing,

our two element interferometer will not be able to separate them; only if the returned signal is dominated by a single scatterer can the interferometry work properly.

The radar receiver forms the cross correlation between the received signal and a copy of the transmitted signal. The strength of the received signal is proportional to the duration of the transmitted pulse. However, a long transmitted pulse will result in poor range resolution. To improve the range resolution, the transmitted signal can be designed so that its autocorrelation function is narrow with low sidelobes. One way to accomplish this is to divide the pulse into segments called bauds and introduce phase shifts of 180 deg for some of the bauds. The most commonly used sequence of phase shifts are Barker codes. The autocorrelation function of a Barker code contains uniformly spaced sidelobes which have a magnitude equal to the reciprocal of the number of bauds and a resolution equal to the width of a single baud.

For this experiment, the transmitted pulse was a 45 km 3 baud Barker code. This has a range resolution of 15 km and sidelobes which are one third of the peak in amplitude (-9.5 dB in power). The wide pulse is used to increase the SNR of the incoherent scatter returns. The trade off is that Barker range sidelobes are now present [*Eaves and Reedy*, 1987]. This will be discussed in more detail in the following section. The interpulse period is 6.6 msec. This allows radial velocities between plus and minus 225 meters per second to be measured unambiguously.

The Measurements

The new radar mode described above was used on many days in September 1996. After looking at measurements from several evenings which contained bottomside spread F, we chose to focus on September 17. This data set displays a wide variety of behavior from very weak bottomside spread F

through violent, rapidly rising plume-type structures. In addition, the new radar mode was particularly effective in producing quality measurements of the motion of both the background ionosphere and the irregularities simultaneously.

Figure Figure 1 is a plot of the received signal power as a function of altitude and time between 20:00 and 23:00. The returns from both the incoherent scatter and the coherent scatter are visible in this plot. Prior to approximately 22:00, the F region irregularities remain between 200 km and 300 km in altitude. Above the irregularities, the weaker incoherent scatter is visible. The power of the incoherent scatter return is proportional to the total number of electrons in the scattering volume. The height of maximum electron density at 20:00 is approximately 310 km. These measurements show that the F region irregularities prior to approximately 22:12 remain below the peak of the layer. From approximately 20:00 to 21:00, the bottomside spread F is comparatively mild and localized in altitude. Between approximately 21:00 and 22:00, the bottomside spread F has strengthened some and now extends to slightly more ranges. After approximately 22:12, the irregularities are no longer confined to the bottomside of the layer. There are three regions in which the irregularities extend upward. The first two regions extend in altitude up to the vicinity of the peak of the layer, the third is considerably more vigorous and extends into the topside of the ionosphere. The third feature would generally be referred to as a plume. The first two features are sometimes called mini-plumes. In the following sections, after discussing measurements of the zonal drift we will discuss estimates of the spatial scales of these features.

As we mentioned previously, Barker sidelobes are present in this data. Power is usually shown in terms of SNR. To make it easier to identify Barker sidelobes, we plot the signal power normalized to the strongest signal measured. In an ideal system, there is no Barker lobe in the adjacent range

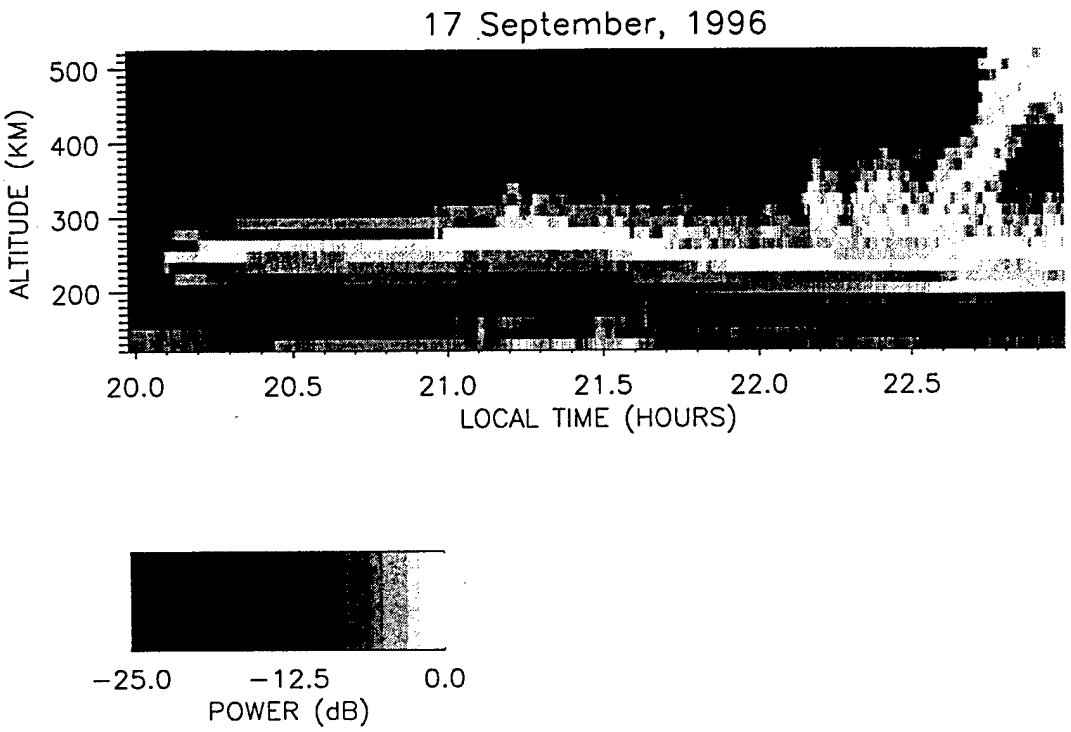

Figure 1: Range Time Intensity plot of measurements made at the Jicamarca Radio Observatory on September 17, 1996 between 20:00 and 23:00 LT. Returns from both coherent and incoherent scatter are visible.

cell, and in the next range cell the response is down 9.5 dB. The effect of the Barker sidelobes is to make the bottomside spread F appear to exist at ranges both above and below its actual location. An unfortunate consequence of this is that incoherent scatter returns from some altitudes on the bottomside of the ionosphere are not available because they are being obscured by the Barker sidelobes.

We shall see that the zonal velocity near the peak of the layer of is roughly 100 meters per second. Using this number, time can be converted into distance. The horizontal and vertical axis in Figure 1 have been adjusted so that the length in the vertical and horizontal directions are plotted on the same scale.

The vertical velocity of the background ionosphere derived from the inco-

herent scatter returns is shown in Figure 2. The velocities shown here were calculated using a five minute coherent integration time and averaging over four range cells, which corresponds to 60 km, centered at 385 km. Positive velocities indicate the ionosphere is rising. The velocities were calculated by using a least squares fitting procedure by Santanu Bhattacharyya which is described in *Bhattacharyya and Kudeki* [1997]. The plot begins approximately three hours before the appearance of the bottomside spread F, and ends at 22:00. After this time the incoherent scatter at these altitudes is no longer available due to the presence of spread F.

With only a brief exception around 19:00 and again at 20:00, the vertical drift is downward. When the drift is downward, the ambient zonal field acts to stabilize the instability. Recall that the growth of the instability is proportional to $E_0 + \frac{g}{\nu_{in}}$ where E_0 is the ambient zonal field normalized by B_0 so that it has units of meters per second. In this case, the instabilities have developed at a height of approximately 250 km and the ambient field for most of the evening acts to stabilize the instability. Overall, the vertical velocities, and the height of the layer are surprisingly low for an evening in which violent, plume-type spread F developed. In subsequent sections we discuss this point in more detail. One interesting feature in the data shown in Figure 1 is the quick rise in altitude of the background ionosphere slightly after 21:00. The vertical velocity at this time as measured from the incoherent scatter is negative and close to zero. This leads us to believe that this feature in the ionosphere was created at some time in the past and is now drifting eastward across the beam.

Due to the presence of spread F, it is not possible to measure the zonal velocity of the background ionosphere on the bottomside of the F layer using incoherent scatter. It is, however, possible to make an estimate of the zonal drift as a function of altitude by calculating the rate of change of the interferometric phase angle of the coherent returns. Figures 3 and 4 show

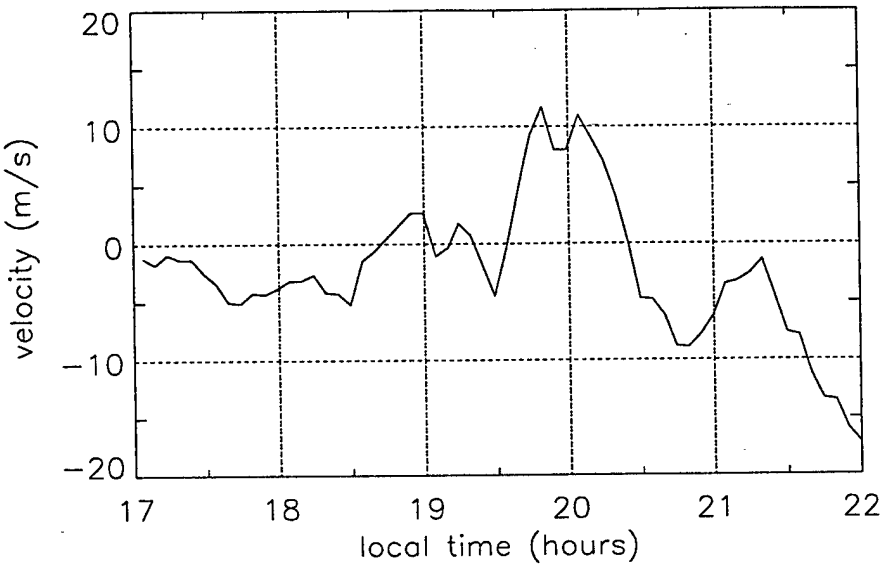

Figure 2: The vertical drift of the background ionosphere as a function of time between 17:00 and 22:00 LT.

the interferometric phase angle as a function of time at ranges between 150 km and 345 km between 21:00 and 22:00 local time.

The normalized cross-spectra were calculated using standard techniques. In each range cell, the cross-spectra were estimated from the output of twelve 64-point DFTs using the standard estimator. The time between estimates of the of the cross-spectra is slightly greater than five seconds. The phases displayed in Figures 3 and 4 have a normalized cross-spectral magnitude greater than 0.7.

If it is the case that a single, small scattering region dominates the received signal for a period of time, as the scatterer moves the interferometric phase angle will change according to the relation $\phi = kdsin(\theta)$, where ϕ is the phase difference between the two antennas, d is the projected baseline in the east-west direction and θ is the angle formed with the vertical. For the geometry of this experiment, the angle θ is small so that $sin(\theta) \approx \theta$, and $\dot{\phi} = kd\dot{\theta}$. The zonal velocity of the scattering region, v, is given by $v = r\dot{\theta}$,

where r is the distance from the radar. Therefore, given the rate of change of the measured phase angle and the distance to the scattering region, the zonal velocity can be estimated.

The data in Figures 3 and 4 show the interferometric phase angle of signals that are highly correlated on the two halves of the antenna as a function of time. At some altitudes, there are very few points and it is not possible to infer a rate of change of the interferometric phase angle. At an altitude of 180 km, with only a couple of brief exceptions, irregularities are not present and the correlation is low in this region. The spatial correlation is also very low in the vicinity of 255 km where the signals are the strongest. Only scatterers that are localized in angle will be highly correlated between the two antennas. From the spatial decorrelation seen at these altitudes we can conclude that the received signals are not coming from a highly localized scattering region.

It is also possible to have so many highly correlated points that a time rate of change of the phase angle cannot be determined. Examples of this type of behavior occur at 210 km and 225 km. At these altitudes, there appear to be many scattering regions and we are not able to estimate a velocity.

When a single scattering region dominates the received signal for a sufficiently long period of time, it forms a feature referred to as a streak. The streak is the progression of the phase angle with time as the scattering region moves across the beam. The slope of the streak is the rate of change of phase with time and is proportional to the velocity of the scattering region. Examples of ranges which contain numerous streaks are 150 km, 165 km, 300 km, 315 km and 330 km. The streaks at these altitudes are well defined and can be used to estimate the zonal drift. The streaks exist at altitudes which are on the upper and lower boundaries of the region containing the irregularities. As the height of the irregularities drops slightly between 21:30 and 22:00 numerous streaks are visible at 300 km, 315 km and 330 km. Note that the slope of the streaks at 150 and 165 km are positive and the slope of

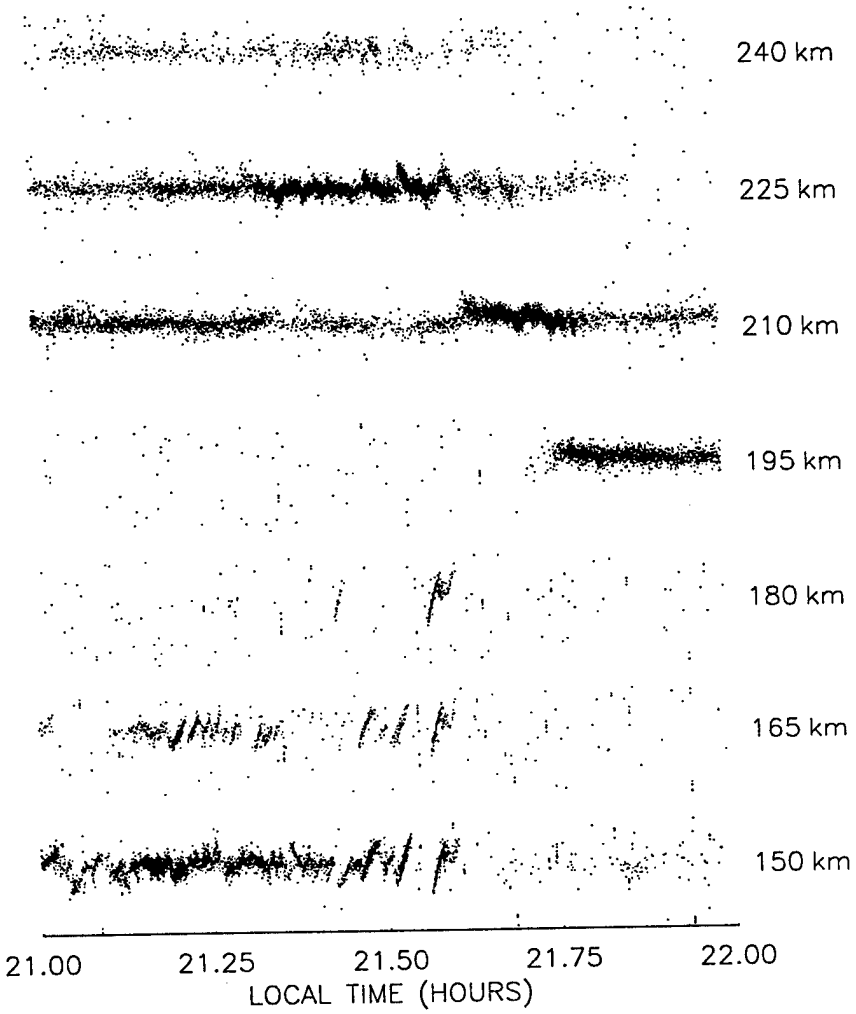

Figure 3: Interferometric phase angle as a function of time for signals having a cross-spectral magnitude greater than 0.7 at altitudes between 150 km and 240 km.

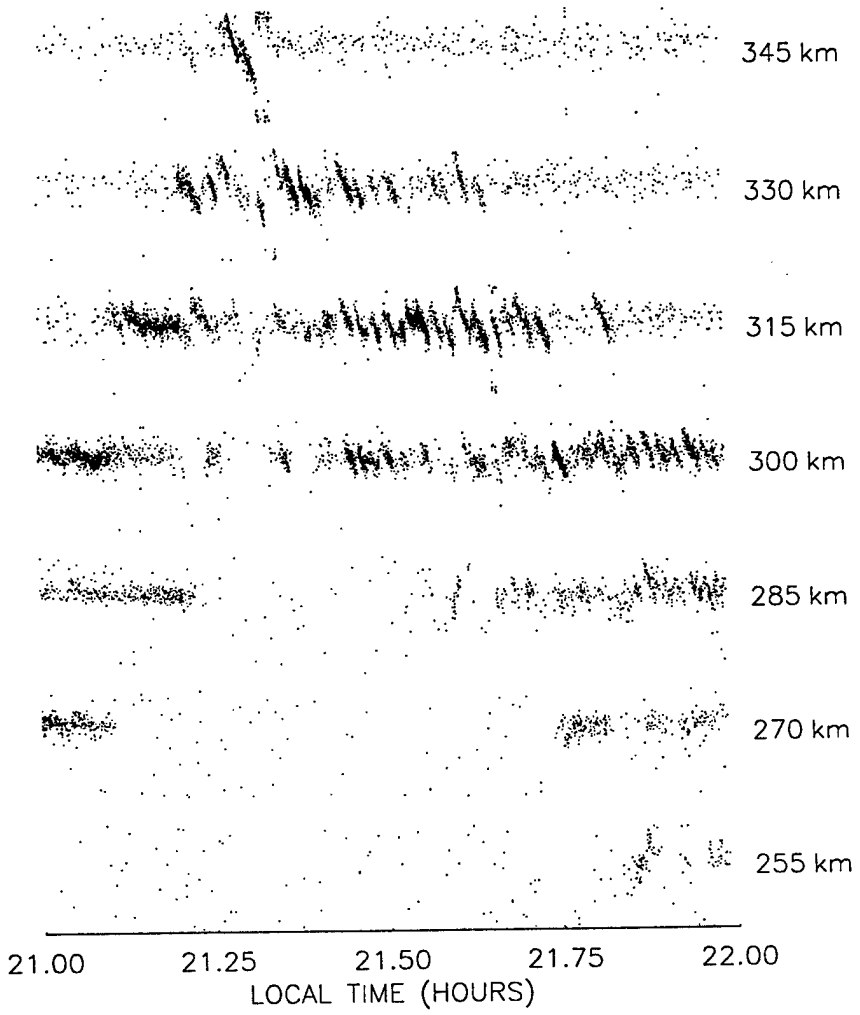

Figure 4: Interferometric phase angle as a function of time for signals having a cross-spectral magnitude greater than 0.7 at altitudes between 255 km and 345 km.

the streaks at 300 km and above are negative. This is because the flow is to the east above and the irregularities, and to the west below the irregularities

An automated process for estimating the zonal velocity was developed and analyzed by Professor Erhan Kudeki and Pinar Zengingönül . A complete description of the method and an analyses which shows that the performance of the algorithm compares favorably with the performance of a least squares fit is given in *Zengingönül* [1996]. The following provides a brief overview of the calculations made to determine the zonal velocity of the irregularities as a function of altitude.

To estimate the zonal velocity, it is necessary to determine the time rate of change of the phase difference between the two antennas. Only samples having a cross-spectral magnitude greater than 0.7 were used in the calculation. The time rate of change of the phase difference between the antennas was estimated by taking the difference between the phase of the cross-spectra at a given Doppler at two different times and dividing by the time difference.

Each estimate of the phase contains some error. To minimize the effect of this error on the calculation, it is desirable to use samples which are separated in time as much as possible. If the time separation between samples is too large, the samples will no longer correspond to the same streak. A time separation of 20 seconds was found to be optimal for our calculations. Figure 5 again shows the interferometric phase angle versus time for samples of the cross-spectra having a cross-spectral magnitude of greater than 0.7. The straight lines overlayed on the plot connect points whose phase difference is used to estimate the velocity. From this plot, we can see that the 20 second separation between points used to estimate the velocity works well: the connected points are a large fraction of the width of a streak and there are no connections between streaks.

The median of the velocity estimates made between 21:00 and 22:00 was calculated at each altitude and the results are shown in Figure 6. This data

shows that there is considerable shear in this region. The existence of such a shear in the irregularities in the equatorial ionosphere has been reported previously by *Kudeki et al.* [1981]. The magnitude of the shear shown in Figure 6 is roughly $8 \times 10^{-4}\ s^{-1}$, which is consistent with the results published in *Kudeki et al.* [1981]. The original question we asked was, does the shear in the horizontal flow have a role in the development of irregularities which exist on the bottomside of the ionosphere for long periods of time? The data presented here are an example of confined bottomside spread F in which a large shear is present. By comparison with our modeling, it is clear that a shear of this magnitude has a significant effect on the development of the instability. It is also possible to infer the horizontal scale size of the irregularities from this data. From the slope of the streaks, we know the drift velocity. The distance between the scatterers is equal to the product of the horizontal velocity and the time between streaks. In Figure 5, for example, the spacing between streaks is typically between one and three minutes and the zonal velocity is estimated to be approximately 70 meters per second. These numbers give a distance between the scattering regions of between 4.2 km and 12.6 km.

Because of the shear, it is difficult to estimate the spatial separation between the three vertically extended features. The altitude at which these features originate appears to be in the vicinity of 250 km. We can get a coarse estimate of the zonal velocity at this altitude by extrapolating from the data shown in Figure 6. This gives the zonal velocity at this altitude to be approximately 20 meters per second. These features are separated in time by approximately 15 minutes. The product of the velocity and the time between features gives a rough estimate of the distance between these events to be on the order of 18 km.

In the regions where the bottomside spread F is strong, the spectra are very broad. An example of this is shown in Figure 7 (b). The spectrum

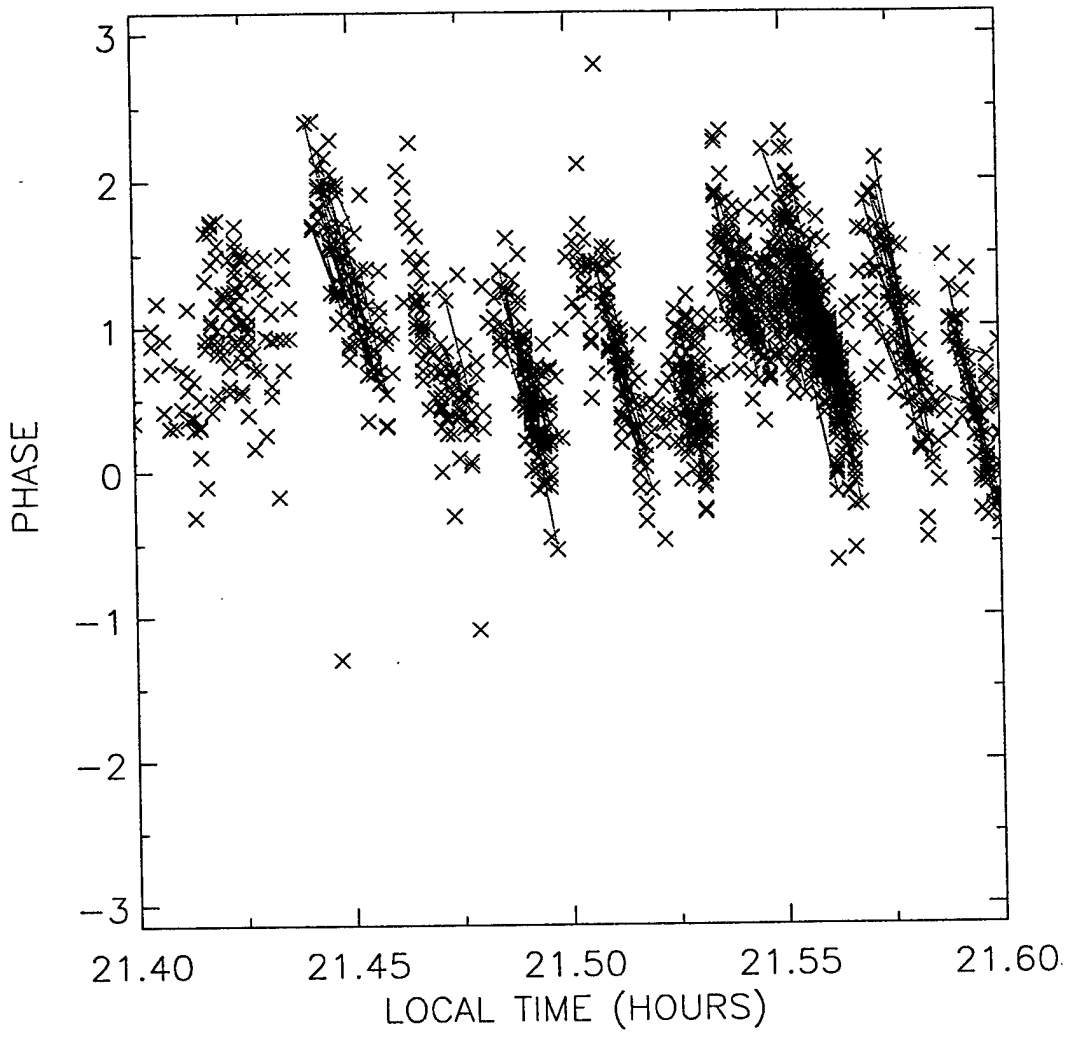

Figure 5: Interferometric phase angle as a function of time for signals having a cross-spectral magnitude greater than 0.7 at 315 km. The straight lines connect pairs of points used to estimate the zonal drift.

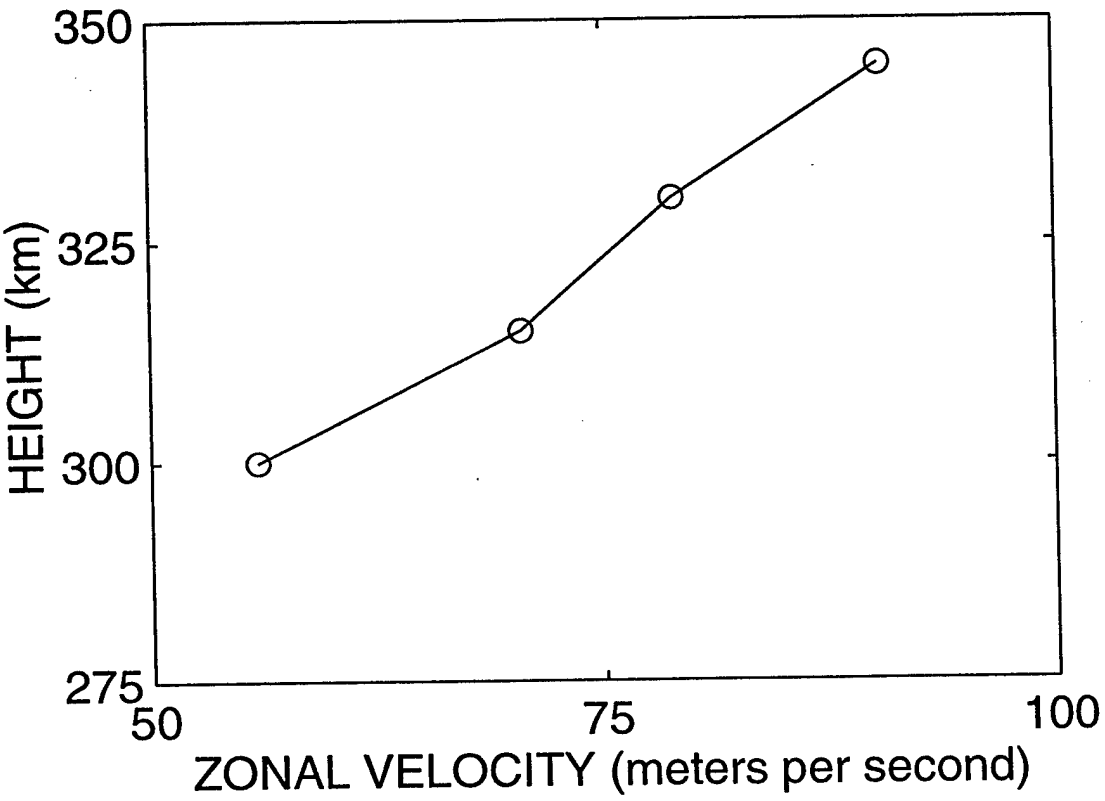

Figure 6: Estimated zonal drifts as a function of altitude.

is clearly aliased and there is no discernible peak. This is representative of the spectra in the regions where the irregularities are the strongest between 255 km and 300 km at times greater than approximately 21:00. This broad spectra could be the result of a very wide distribution of radial velocities (in excess of 450 meters per second). However, if this is the case, it is interesting that the altitude of the irregularities is neither rapidly rising nor rapidly descending. In fact, the height of the irregular region moves very little prior to the rapid rise in altitude after 22:00. The broad spectra could also be the result of complicated motions in the bottomside which result in very short lifetimes (less than five msec) for the scattering sources of the VHF energy. It is interesting to note that, as we showed in Figures 2 and 3, the spatial correlation of the returns from these regions is also very low. Clearly, our measurements are not sophisticated enough to characterize the complicated motion in these regions.

Both above and below the region where the signals are the strongest, the spectra are typically not as broad. An example of this is shown in Figure 7 (a) which shows the spectrum at 21:30 at 225 km altitude. There is a distinct peak in the spectrum which is located close to zero velocity. As is sometimes the case, there is also a very broad component to the spectrum which is on the order of 10 dB below the peak response. At this altitude, as can be seen in Figure 2, the magnitude of the spatial correlation is much higher than at 255 km. In fact, in this region, there are so many highly correlated points that it is not possible to identify any streaks.

After 23:00, the appearance of the irregularities changes dramatically. The system has evolved very quickly, and the irregularities are no longer confined to the bottomside of the layer. Three distinct regions of plasma irregularities which extend into the height of the most dense ionization are visible (see Figure 1). These features are separated in time by about 15 minutes. Figure 8 shows an example spectrum taken from each of these

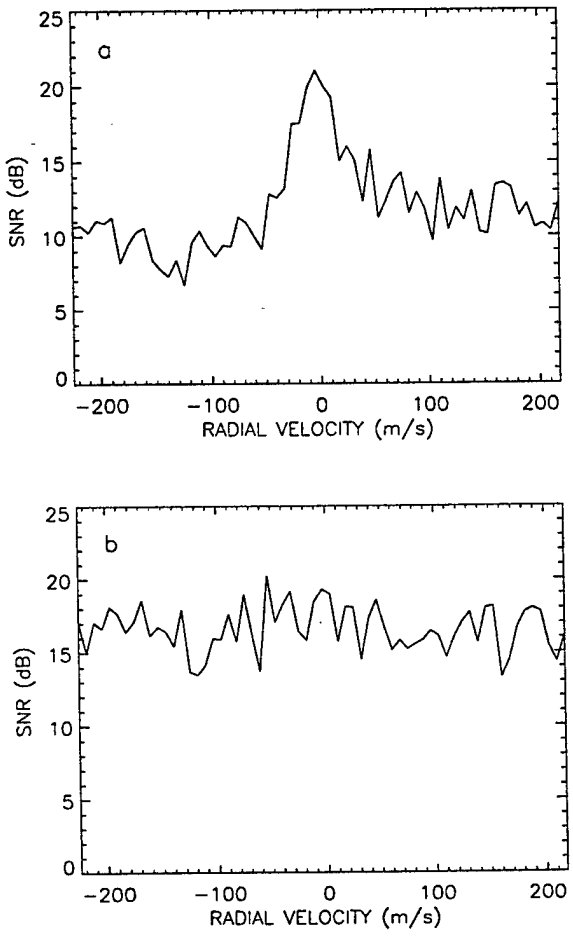

Figure 7: The spectrum of bottomside spread F at 21:30 at (a) 225 km and (b) 255 km. (a) is representative of the spectra near the edge of the irregularities. (b) is representative of the regions where the spread F is the strongest.

regions at an altitude of 360 km. The spectra of the first two features shown in Figures 8 (a) and 8 (b) are comparatively narrow and located close to zero Doppler. In Figure 8 (b), there is again a very broad component of the spectrum which is on the order of 10 dB below the maximum in the response. From this data, it appears that the irregularities in this region are not moving rapidly in the vertical direction.

The third of the three vertically oriented features is considerably different than the first two. The first two features extend into the vicinity of the peak of the ionosphere, the third extends well into the topside of the layer. An example spectrum from the third feature is shown in Figure 8 (c). The majority of the energy in the spectrum is at Dopplers corresponding to radial velocities between 100 meters per second and 200 meters per second. There is some energy at less than 100 meters per second and at greater than 225 meters per second that has wrapped around to the negative Dopplers. From this data, we can infer that the plasma is being rapidly advected from the bottomside of the layer into the topside at velocities which are in excess of 100 meters per second.

These data show that the behavior of the bottomside spread F can change very quickly. Between 22:00 and 23:00, we see confined bottomside spread F, two mini plumes which have risen up to the height of the peak of the F layer which appear to no longer be rising, a very violent plume structure and finally more confined bottomside spread F.

Discussion

It is generally accepted that irregularities in the F region of the equatorial ionosphere are produced by the Rayleigh-Taylor instability. As is discussed in *Kelley* [1989], if the mitigating effect of the shear and the diffusion are neglected, the growth rate of the linearized model for the instability is given

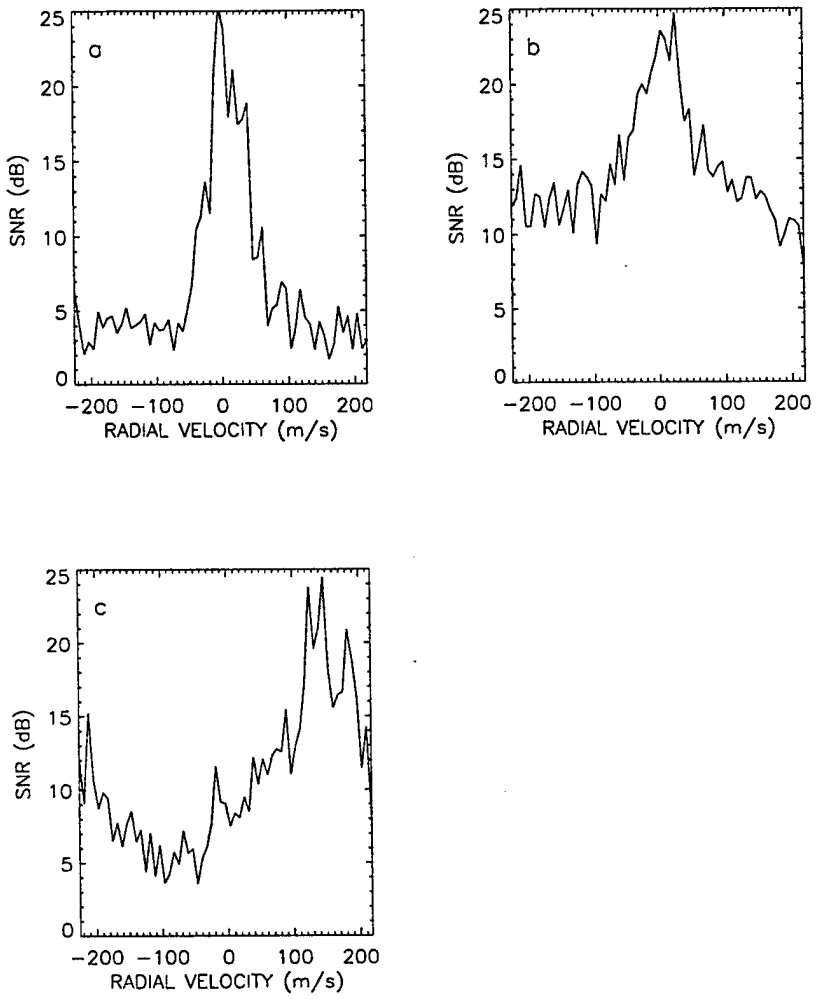

Figure 8: Representative spectra from the three plume-type structures which drifted past Jicamarca after 22:00 LT. The measurements were made at an altitude of 360 km at (a) 22:15, (b) 22:30 and (c) 22:52.

by $(E_0+\frac{g}{\nu_{in}})L_n{}^{-1}$, where E_0 is the eastward component of the ambient electric field normalized by the value of the Earth's magnetic field so that it has units of velocity, ν_{in} is the ion neutral collision frequency and L_n is the gradient scale length. As can be seen from this expression, a westward ambient zonal field (downward drift) acts to stabilize the instability, and the effect of gravity is strongly dependent on altitude due to the presence of the ion neutral collision frequency. With the exception of a brief period which coincided with the appearance of the irregularities, the vertical drift on the evening of September 17, 1996 is close to zero or downward.

On September 17, 1996, bottomside F region irregularities developed at an altitude of approximately 250 km and the ambient zonal field was predominantly westward (see Figure 2). At first glance, it is surprising that irregularities would develop at an altitude this low without a significant eastward electric field. This was not an isolated instance, however, and similar behavior was seen on several days during the fall 1996 MISETA campaign. In the following section, we consider this apparent discrepancy in detail and suggest a potential additional source for instability that is not accounted for in the linearized growth rate stated above.

To calculate the growth rate predicted by the linearized model stated in the preceding section, it is necessary to have an estimate of the ion-neutral collision frequency in the region where the instabilities developed. The ion-neutral collision frequency is a function of the neutral density and the temperature. At 250 km altitude the MSIS model predicts the neutral density on this day to be 1.07×10^9 cm^{-3} and the temperature to be 705 Kelvin. Using these numbers in the expression for the ion-neutral collision frequency derived in *Pesnell et al.* [1993], we calculated the collision frequency to be $0.73\ s^{-1}$.

We do not have a measurement of the gradient scale length of the background ionosphere at the times of interest. A typical number is 20 km. For

the collision frequency derived above and an ambient zonal field which corresponds to a vertical drift of -5 meters per second, the time for the amplitude of the instability to grow by a factor of e is more than 40 minutes. And this estimate neglects diffusion and the effect of the shear, both of which will decrease the growth rate. Between 20:30 and 21:30 the average vertical drift is less than -5 meters per second. Based on the linearized growth rate, we would expect the instability to grow by slightly more than a factor of e between 20:30 and 21:30. For times after approximately 21:30, the stabilizing effect of the ambient electric field is larger than the de-stabilizing effect of gravity. At these times, the growth rate is negative and the irregularities, as predicted by linear theory, are decaying.

These predictions for the development of the instability do not appear to agree with the behavior that was observed. At 20:30, the bottomside irregularities have recently appeared and exist in only a very narrow region in altitude. (The response at close to 300 km is a Barker sidelobe.) By 22:00, the instability has extended in altitude and grown to a sufficiently large amplitude that nonlinear effects have become important and plume-type structures are beginning to appear. This development is not consistent with the instability growing by a factor of e. This leads us to ask, are there any possible additional sources of instability that have not been accounted for in the derivation of the linearized growth rate?

In work that will be published in the near future, we derived a model for the evolution of the generalized Rayleigh-Taylor instability which includes an inhomogeneous vertical electric field. An important feature of the model was that the ambient vertical electric field was constructed so as to satisfy the relation $\nabla \cdot [n_0(z)E_z(z)\hat{z}] = 0$, which implies that the product $n_0(z)E_z(z)$ is equal to a constant. Since $n_0(z)$ is always greater than zero, the sign of $E_z(z)$ cannot change. Consequently, the flow should be either to the west at all altitudes or to the east at all altitudes.

It is well known, however, that the zonal flow in the equatorial ionosphere is to the west at low altitudes, and to the east at high altitudes. The current understanding of the origin of the shear is that the flow of the background ionosphere at low altitudes is controlled by E-region dynamo and the flow at higher altitudes is controlled by the F-region dynamo. An observation that has not been discussed in the past is that the altitude where the flow reverses appears to coincide with the height at which the instabilities first develop. This observation was first made by the staff at the Jicamarca Radio Observatory (private communication, Erhan Kudeki, 1996).

The data in Figure 3 show the flow to be clearly to the west at altitudes as high as 180 km, and at 300 km, the flow is to the east. Instabilities are present at the altitudes between these two regions, but, as was discussed previously, we cannot determine the direction of the flow in this region. Prior to 21:00, strong returns from irregularities were seen at altitudes as low as 210 km. From this data, it appears probable that instabilities are present at altitudes in the vicinity of where the flow has reversed. Estimates of the zonal drift are not available when the instability first developed, so that from this data we cannot determine if it is indeed true that the irregularities have first developed where the flow changed direction.

A reversal in the direction of the flow represents a significant difference from the standard model. At the altitude where the flow reverses, there is a divergence in the vertical Pederson current. To satisfy the requirement that quasineutrality be maintained, a current must be created in either the zonal direction or along the magnetic field. If a current were created in the zonal direction, this could produce instability in the same manner as the ion Pederson current which results from the ambient zonal field, or gravity which is the source of the generalized Rayleigh-Taylor instability.

If we introduce an electrostatic perturbation to represent a possible electric field to drive a Pederson current in the zonal direction to satisfy div **J**

equal to zero when there are no density perturbations, the expression for the divergence of **J** becomes $\nabla \cdot [n_0(z)(E_z(z) - \nabla\phi)] = 0$. We can solve this equation for ϕ, and as we have stated previously this solution is unique. The solution of this equation, however, is that the total electric field, i.e. $E_z(z) - \nabla\phi$, be proportional to the reciprocal of $n_0(z)$. This solution implies that a perturbation electric field is generated which results in flow only in one direction. This proves that there is no ambient electric field profile that can satisfy the potential equation and produce a reversal in the flow.

One thought is that perhaps the addition of Hall currents might allow the divergence of **J** equal to zero to be satisfied. However, this cannot be the case because the divergence of a Hall current resulting from a vertical electric field in an ionosphere which has no variations in the horizontal direction is zero.

If we introduce small perturbations to the density and solve the system numerically, we get a solution which corresponds to the solution described above and again the resulting flow is only in one direction.

This leads us to consider how the model could be different such that a reversal in the flow and a divergence free Pederson current can both be present. One possibility is that the assumption of a vertically stratified ionosphere is not correct. If significant horizontal variations in the structure of the ionosphere were present, it may be possible for a two dimensional current system to satisfy the system. It may also be possible that Hall currents play a role here even though the Hall conductivity is more than two orders of magnitude smaller than the Pederson conductivity.

Another possibility is that the system is fundamentally three-dimensional and significant currents are being generated along the magnetic field. The existence of field aligned currents associated with bottomside spread F has been discussed by *Vickrey et al.* [1984] in connection with the formation of images in the F region valley. Field aligned currents in the presence of a den-

sity gradient can produce irregularities through a mechanism known as the current convective instability. Initial estimates of the growth of this instability were made using expressions derived in *Ossakow and Chaturvedi* [1979]. The results of these calculations lead us to believe that it is unlikely that this instability is the source of the observed irregularities in the bottomside of the F region.

It is interesting to note that even in the presence of a considerable shear, the two mini plumes are oriented essentially vertically. If these had existed for any significant period of time prior to drifting past the Jicamarca observatory, we would expect that the higher altitudes would have drifted farther east than the lower altitudes. There is some evidence of this in the full-blown plume which follows closely behind these mini plumes. One possible explanation is that these features have developed very rapidly just prior to drifting past Jicamarca, another is that conditions have changed and the shear has been reduced. However, since it is no longer possible to identify streaks in the data after 22:00, we cannot make an estimate of the shear in this region.

When the irregularities were confined to the bottomside of the layer, a large shear was measured. When the irregularities were driven upwards, the structure of the instabilities leads us to believe that either very large perturbation fields were produced, or the shear decreased significantly. In either case, the shear is no longer effective in stretching the irregularities and then removing them by diffusion. For these features the effect of the shear is no longer important.

Conclusions

In this report, we have presented radar measurements from a three hour period during which bottomside spread F was observed. The measurements were made using a new radar mode which provided high quality estimates of

the drift of the background ionosphere and simultaneous measurement of the motion of the plasma irregularities. Our numerical modeling efforts, which will be published in the near future, were motivated by the question, does a sheared horizontal flow have a significant role in confining irregularities to the bottomside of the F region? The measurements presented here show that a considerable shear was present when confined, bottomside irregularities were observed. Based on our numerical models, it is clear that a shear of this magnitude will have a considerable effect on the development of the irregularities.

A surprising result is that the growth of the bottomside irregularities appears to be much faster than predicted by the well-known expression for the growth of the linearized system without shear. We believe that this experimental evidence suggests that there may be other sources of instability that are not included in the well-known linear model for the system. Based on the measurements of the zonal motion of the irregularities, we have noticed that the divergence in the vertical Pederson current associated with the background ionosphere may be a possible additional source of instability.

References

Bhattacharyya, S., and E. Kudeki, Plasma drift measurements at Jicamarca during the development of equatorial spread F, *J. Geophys. Res., to be submitted*, 1997.

Eaves, J., and E. Reedy, *Principles of Modern Radar*, Van Nostrand Reinhold, New York, 1987.

Kelley, M. C., *The Earth's Ionosphere*, Academic, San Diego, Calif., 1989.

Kudeki, E., and S. Bhattacharyya, Incoherent scatter F-region drift measurements at Jicamarca, *J. Geophys. Res., to be submitted*, 1997.

Kudeki, E., B. G. Fejer, D. T. Farley, and H. M. Ierkic, Interferometer studies of equatorial *F* region irregularities and drifts, *Geophys. Res. Lett.*, *8*, 377, 1981.

Ossakow, S. L., and P. K. Chaturvedi, Current convective instability in the diffuse

aurora, *Geophys. Res. Lett.*, *6*, 332, 1979.

Pesnell, W. D., K. Omidvar, and W. R. Hoegy, Momentum transfer collision frequency of $O^+ - O$, *Geophys. Res. Lett.*, *20*, 1343, 1993.

Vickrey, J. F., M. C. Kelley, R. Pfaff, and S. Goldman, Low-altitude image striations associated with bottomside spread F: observations and theory, *J. Geophys. Res.*, *89*, 2955, 1984.

Woodman, R., and T. Hagfors, Methods for the measurement of vertical motions near the magnetic equator by incoherent scattering, *J. Geophys. Res.*, *74*, 1205, 1969.

Zengingönül, H. P., *A Study on Several Radar Techniques Used for the Estimation of Ionospheric Plasma Drifts.* PhD thesis, University of Illinois, Champaign Il., 1996.

Appendix B

Progress Report:

Installation of Cornell Airglow Imager in Maui

Progress Report:

Installation of Cornell Airglow Imager in Maui

July 28, 1997

Craig T. Palmer
3821 Walt Ann Dr.
Ellicott City, MD 21042
(410) 531-2065
palmer@ee.cornell.edu

Overview

On June 17, 1997 and June 20, 1997 I investigated installing the Cornell Airglow Imager on Mt. Haleakala in Maui, Hawaii. This report will summarize what I learned, who I talked to, and what decisions were made. When I say "we" in this document, I am referring to the Cornell Airglow Team led by Dr. Mike Kelley.

The facility on top of Mt. Haleakala (10,000 ft.) is the Maui Space Surveillance System (MSSS). The MSSS Observatory includes the Air Force Maui Optical Station (AMOS, Phillips Laboratory), much of which is operated by Rockwell Power Systems. In this document I will refer to the mountain top facility as "AMOS Haleakala." The technical and administrative support facility is located in the Maui Research and Technology Park in Kihei. This park is on the coast of Maui below Mt. Haleakala. I will refer to this support facility as "AMOS Kihei." Across the street from AMOS Kihei is the Maui High Performance Computing Center (MHPCC), which has some ties to AMOS. Details on AMOS can be found at their web site (http://ulua.mhpcc.edu/amos.html) or in the AMOS User's Manual.

Paul Kervin was my initial contact at AMOS, whom Mike Kelley has been working with to establish a remote site for our imager. From Paul I was lead to John Africano, and ultimately Jack Albetski became the responsible engineer for our experiment (see Appendix A for contact information). On Tuesday, June 17 I first met with Jack, Paul, and John at AMOS Kihei. Here we discussed the goals of our experiment and started to get into the details of how they will be achieved.

As seen in the MSSS (AMOS) Visiting Experimenter's Initial Contact Survey Form, the primary goal is to obtain images of gravity waves in ionosphere airglow layers and to determine their origins. This will be achieved by installing high quality CCD camera on top of Mt. Haleakala. The primary tasks we would like AMOS to accomplish are (1) provide location for camera and computer installation, (2) provide Internet access to computer and (3) provide a small amount of technician time for the experiment. We will provide a large case which will contain the camera and be mounted on the roof. We will also provide the computer to which the camera is connected. The estimated start date is between November 1997 and May 1998. Duration is 3 years to indefinite. A roughly estimated budget for this effort is $3,000/yr. plus installation cost.

On Tuesday afternoon, Jack and I went up to AMOS Haleakala and investigated where we could physically install the camera and computer. See the section titled "Camera Installation" for details.

On Friday, June 20, we once again met at AMOS Kihei, this time the attendance was myself, Mike Kelley, Paul Kervin, Jack Albetski, and John Africano. Here we presented the best installation option and confirmed that we are ready to move forward in the process.

The next step in the process is for Jack and Paul to establish a ROM (Rough Order of Magnitude) cost estimate. I believe this will be followed by an "Approval to Plan" request. Phillips Laboratory needs to give this approval, which involves responses from Major Richards and Major Simmons. We are currently waiting for a reply from AMOS, but are pretty confident it will go through and should start preparing to install the camera in Maui.

Camera Installation

There were several options for where to install the camera case and computer. I will present the preferred option here, but alternate locations are sited in Appendix B.

The camera will be mounted in a large (approx. 30" x 30" x 42" high) weather-proof case. The camera electronics unit and cooling unit will also be in the case. The camera will be mounted vertically, with the top all-sky lens extending just beyond the top of the case, covered with a transparent dome. The approximate weight of the case and its contents is 150 pounds. Three cables will interface to the case: a power cable, serial data cable, and Photometrics camera controller cable. The power cable will go to a UPS on a standard 115Vac line. The other two cables will connect to the computer.

The camera case will be installed outside on the roof of a 8'x20' trailer, referred to as the alignment trailer, next to the LBD dome. The computer will be housed inside that trailer, providing close, easy access to the camera. Figure 1 shows a sketch of the setup. A mounting bracket will be secured just above the roof of the trailer, anchoring to the metal beams inside the trailer. The bracket will be installed over the two beams furthest north. Detailed specifications for this bracket will be given to AMOS by Cornell to allow it to fit a matching bracket on the bottom of the camera case. AMOS will arrange for the trailer bracket to be installed before we arrive with the camera case. Cornell will obtain a case, install a bracket on the bottom of the case, a dome on the top, brackets inside the case to secure the camera, and a connecting plate for the cables to attach to. Appendix C contains details on the trailer structure, mounting brackets and the camera case. A ladder or some other structure will be required to access the roof of the trailer. A walkway (approx. 2.5 ft wide) surrounds the trailer and is about 10 ft below the roof. A simple step-ladder could be used, or a ladder could be permanently attached to the side of the trailer. Because it will be rare that anyone actually has to go on the roof, a stepladder stored inside the trailer may be the best option.

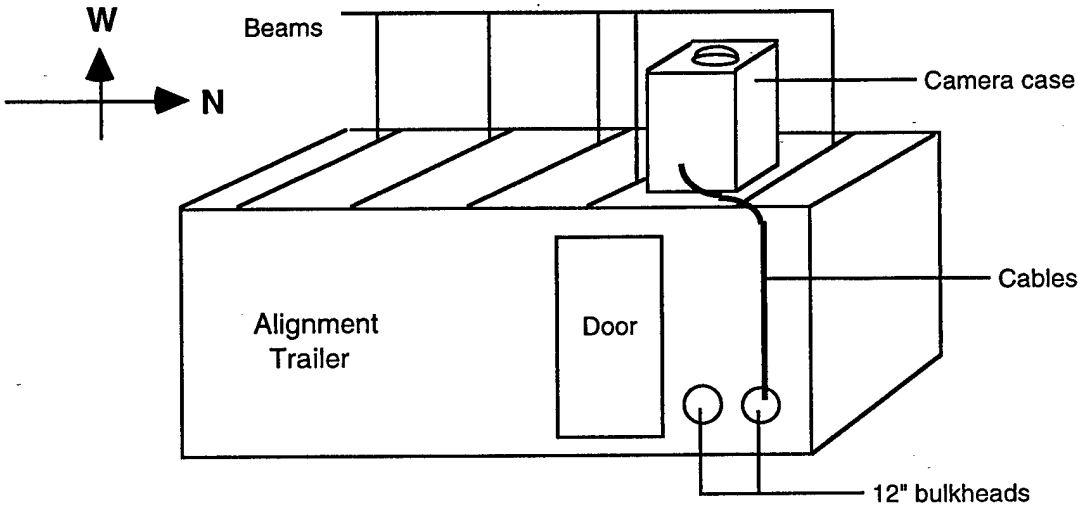

Figure 1: Camera installation sketch. Camera case is mounted on top of alignment trailer next to the LBD dome. Cables run down the trailer and through the bulkhead. Computer is housed inside the trailer.

The cables from the case will pass across the roof of the trailer to the north-east corner, and down the east wall to one of the 12" bulkheads on the lower side of the east wall. The cables will then pass through the bulkhead into the trailer where the computer and UPS will be installed. A 12" diameter plate will be made to allow the cables to pass through the bulkhead, while still being watertight and semi-airtight. It is undecided if this plate will be provided by Cornell or AMOS. A possible simple solution would be two 12" diameter semi-circles, with a notch cut out of the middle just larger than the cable group. These semi-circles could be aligned and sealed with two plates as shown in Figure 2a. Two semi-circles are preferred over a single circle with a hole in the middle because the inside hole would have to be almost 4" wide to accommodate the cable connector on the Photometrics cable. Another option is a single 12" diameter plate, with a 4" x 1" rectangular hole in the middle large enough for the connectors to pass through (Figure 2b). This hole could then be sealed over by another plate with just enough clearance for the cable group. A more sophisticated (although possibly overkill) option would be to provide jacks on the 12" plate that the cables could plug in to, rather than passing through. On the inside of plate, jacks would be provided that connect through to the computer.

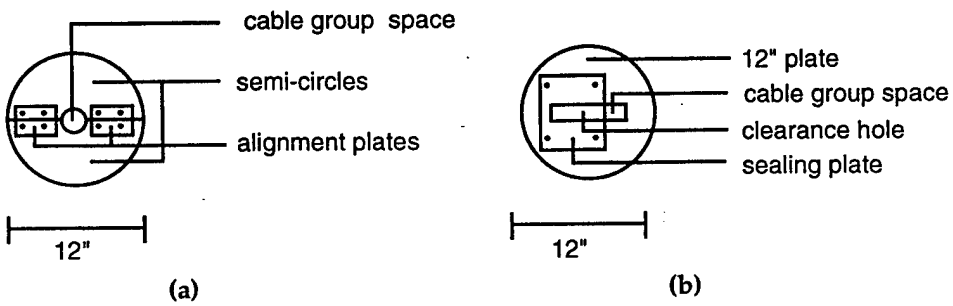

Figure 2: 12" diameter bulkhead cover with cable passage.

It would be good to protect the exterior cables running from the camera case to the bulkhead from the weather and strong ultra-violet rays. This could be done with a conduit or some other casing. Perhaps a 2" square conduit with a cover would be best, allowing us to lay the wires in then cover it. The large (almost 4") connector on the Photometrics cable prevents us from feeding the wires through a 2" conduit pipe. Once inside the trailer, we only require approximately three square feet of desk space for the computer. Currently, this could easily fit in the north-east corner of the trailer, right next to the bulkhead and beside the door. The approximate cable lengths for this setup are:

6 ft from case to edge of roof
8 ft from roof to 12" bulkhead
4 ft from bulkhead to computer
5 ft reserve slack
---
23 ft total

23 feet is well within the maximum length of the cables (much shorter than the current length in use in Arecibo).

Because the trailer is isolated on the roof of the AMOS building, several external connections will be required between the trailer and the building. Those connections are power, Internet, and phone. We will leave the installation of those lines completely up to AMOS, as they know best how to work with their existing infrastructure. There are already power cables entering the trailer, but they were not hot in June. It may be as simple as a circuit breaker, but we did not investigate that.

The alternate installation plan is to keep the camera on the trailer roof, but house the computer inside the main building instead of in the trailer. There are many advantages to the plan we chose. I already discussed the short wire length between the camera case and the computer. In the alternate plan, the cables would be at least 75 feet. In addition to having short cables, it is convenient to have the computer close to the camera for on-site testing when

we visit AMOS, or when we have a technician perform tests for us. Third, the cable installation is much simpler than if the computer was in the main building. Finally, the room where the computer would be located if we used the alternate plan is permanently secured for classified military work. This would mean that whenever we were on site to work with the camera, we would have to have an escort with us the entire time we are using the computer. By storing the computer in the trailer, we essentially have our own office space that will keep us out of the way of permanent AMOS experiments and will assure our system is untouched when we are gone. On the same note, the major disadvantage to this plan is the accessibility of the system. If we call AMOS Haleakala wanting a simple check on the computer, the technician/helper has to find his way to the roof, cross the roof to the trailer and unlock the trailer. If the computer was housed in the main building it would be much simpler. We have been assured, however, that this disadvantage will not be a problem, and on the rare occasion when we need that kind of assistance we will be able to work it out. Concerns were discussed about walking on the roof of the main building because of a waterproof liner, but rubber walkways have been laid down protecting that liner and AMOS engineers have stated that walking there would not pose a problem.

Network Communications

I spoke to Dean Ikioka, an AMOS network engineer, about communication issues. I had several concerns. First, are we going to run into trouble with classified networks? The answer is no, because there is an unclassified network at AMOS Haleakala that also runs down to AMOS Kihei that Cornell will be able to use for communicating with the camera. My other question regarded sending our images back to Cornell in near real time. I told Dean that we will be interested in sending data on the order of 250 Mbytes per night. He said that it would not be a problem. He felt that we would not be bogged down by their network usage and that our transmission would not bog down their network; in other words neither of us will interfere with the other. Based on our experience in Arecibo I tried to be as thorough as possible in making sure this would not be a problem and Dean was very confident that it would not be.

The current link between AMOS Haleakala and AMOS Kihei is a T1 microwave link, but within a year should be upgraded to a T3 fiber optic line. Transmission from AMOS Haleakala to Cornell would use this link, and possibly get routed through MHPCC.

When I was at AMOS Haleakala I tested standard FTP transmissions from a Macintosh on the unclassified network to our Macintosh at Cornell (papaya). I was very pleased with the results, which implied that near real time transmission of the images will be possible, and almost certainly daily

transmission in the worst case. The test was run at 5:45pm Hawaii time on a JPL computer using Fetch. Paul Sidney is known as the "Mac Guy" at AMOS Haleakala and I believe is in charge of that computer. At the time Kevin Moore, a night manager, was helping me. The TCP settings for the computer were as follows:

IP Address	205.149.123.53	
Domain Name Server	204.107.237.26	mhpcc.af.mil
Gateway	205.149.123.130	

I transmitted single images (approx. 500 Kbytes). Transmission rates were typically around 14K to 17K bytes/sec, sometimes going as high as 19K, resulting in image transmission times around 30 seconds.

Given an average exposure time of more than 50 seconds ((90 sec + 90 sec + 90 sec + 1 sec + 8 sec)/5 = 55 sec) plus overhead implies that when the network is running smoothly we will be able to transmit each image after it is acquired and the next image is being exposed. Also, the images could be compressed allowing even faster transmission time. Another way to look at the transmission feasibility is to look at complete cycles. With five uncompressed images per cycle, we have 2.5 Mbytes, or approximately 2.5 minutes of transmission time. The cycle takes approximately 7 minutes to complete, so we should have a reserve of 4.5 minutes.

I would still recommend saving the images to disk, keeping a one night backup. If for some reason the images were unable to be transmitted real time, there will be plenty of time during the day to transmit the images back to Cornell. Once confirmation is made that the images arrived at Cornell, the AMOS Haleakala storage can be cleared.

It would be interesting to do some analysis on the link between Cornell and AMOS Haleakala. Particularly finding out where the slowest link between papaya and the Macintosh in Maui is and what time of day is best.

Weather

Weather conditions on top of Haleakala (10,000 ft) are typically 30° cooler than in Kihei and can experience very high winds (125 mph highest recently recorded). High and low temperatures on the mountain over a five year period were 21°C (70°F) maximum and -7°C (19°F) minimum. Marine haze and clouds are usually well below the observatory, giving dry, clear air. AMOS said they typically find the following viewing conditions for their experiments: 50% photometric, 25% spectroscopic, and 25% down due to weather. Details on the temperature, wind, and cloud cover can be found on their web site (http://ulua.mhpcc.edu/amos.html) or the AMOS User's Manual.

Live All-Sky Images for AMOS

AMOS has interest in obtaining live all-sky images from Haleakala to detect cirrus clouds. Currently, one of our filter positions is "NONE" (no filter at all). This position is useful for checking cloud cover. The period of our images is approximately 7 minutes. By saving the NONE images to a location where AMOS can get to them, they can view the most recent all-sky image (note the camera is only run at night on a dark sky to prevent overexposure). One issue that needs to be addressed is the image viewer. If the images are saved as JPEG or GIF, most any viewer can read them. If they are in our special IMC format, we would need to provide an ImagePlayer for them to use. Most of their computers are Mac's, DEC's, or Silicon Graphics.

Miscellaneous

During our meetings AMOS asked if we had an official experiment name. With a name like Cornell Ionospheric Airglow, CIA is a natural acronym, but we may not get that past the Air Force! Another name could be Cornell Airglow Imager, etc. I don't think the experiment name is critical, but something to think about.

A rough idea of power requirements may be necessary. We know the maximum power based on our two UPS modules running the entire system in Arecibo. Also, on the topic of UPS's, it may be cheaper to buy new modules in Maui than to ship our current modules to Maui (I also am not sure if we ever bought the original UPS from Arecibo; Paul Castleberg installed it for us). There is a K-Mart near the airport, or a Cost-Co (a membership warehouse), both of which are possibilities for buying such equipment.

A possible concern is heat buildup inside the camera case. Sources for this heat are internal electronics, the heat exchanger for the cooling unit, and solar radiation. The exterior of the case will be white, so most solar radiation should be reflected away. However the hole under the dome will allow some solar rays to enter the case. After an initial investigation I do not believe the heat will be a problem. We are fortunate that the maximum temperature on the mountain top is only 70°F. I do feel that we need to look into this situation a little closer. We can determine the total amount of power used by the equipment in the case, and estimate the maximum heat dissipation in watts. We may also want to power down the units inside the case during the day (the only time heat should be a problem). More sophisticated ideas include installing an internal temperature gage, with an automatic shut-off at high temperatures. Or installing a small air conditioner on the side of the case, which are sold by certain case companies.

We discussed contracting a small amount of technician time, on the order of 6 hours per month. That does not seem to be a problem and will be arranged at a later date.

In Arecibo we use a hair dryer to heat the inside of the camera dome, thus preventing moisture condensation on the outside of the dome. Because of the cool outside temperature at Haleakala, we may have the opposite problem. To make sure there is no moisture on the inside of the dome, we may want to use desiccant inside the case to absorb all the moisture. I do not know how much you would need to keep that whole area dry. A more extreme measure would be a dry nitrogen purge. We also need to make sure the case is completely water and air tight. As a whole, however, Haleakala is very dry and should be much easier to deal with than the tropics of Arecibo.

Dr. Doug Curie at University of Maryland in Astronomy had an all-sky camera in Maui years ago and may be a good reference.

Appendix A: Contacts

Cornell Airglow Team

Craig Palmer
palmer@ee.cornell.edu
(410) 531-2065
3821 Walt Ann Dr.
Ellicott City, MD 21042

Dr. Mike Kelley
mikek@ee.cornell.edu
(607) 255-7425
304 Rhodes Hall
Cornell University
Ithaca, NY 14853

Stan Leong
scl2@cornell.edu
(607) 255-8298

Francisco Garcia
fgarcia@ee.cornell.edu
(607) 255-8298

AMOS

John Africano
(808) 874-1579

Jack Albetski
jalbetski@premier.mhpcc.af.mil
(808) 874-1571

Paul Kervin
kervin@eagle.mhpcc.af.mil
(808) 874-1542
(808) 874-1600 fax

Dean Ikioka
AMOS Kihei
Network communications

Phillips Laboratory - AMOS
535 Lipoa Parkway, Suite 200
Kihei, Maui, HI 96753

Appendix B: Alternate Installation Location

While the camera installation presented in the main part of this document is highly preferred, we strongly considered an alternate plan before we decided. This plan would again mount the camera case to the roof of the alignment trailer next to the LBD dome. The cables from the case would then pass down the trailer and across a short section of the building roof into a plate on the bottom portion of the LBD dome. A plate measuring 13.5" x 11.5" already exists and would be easily modified to allow our cables to pass through. The cables would then go through the LBD room (Room 47) and into Room 20, where Don Ruffatto's office is. There is a corner in the far end of Room 20 where Don agreed it would be okay to put the computer.

Cable requirements are as follows:

6 ft along roof of trailer (assuming case is at south end. Add 12 ft if case is mounted in the north end, where original plan specifies.)
14 ft from trailer roof to main building roof
6 ft along roof to LBD dome
7 ft down from dome into building
9 ft across LBD room (Rm. 47)
8 ft across LBD room
19 ft across Room 20
6 ft down to computer

---

75 ft Total (87 ft if camera case is installed at north end of trailer)

These cable lengths, 75 ft or probably 87 ft, are pushing the specifications on the Photometrics cable maximum length. It may be possible to get boosters if this is a problem. Alan Lichty at Photometrics has more details on maximum cable lengths.

A summary of advantages and disadvantages is almost the opposite as those listed for the primary installation plan. Advantage: computer close to AMOS employees. Disadvantages: long cable lengths, classified location of computer (escort required), unprotected computer.

Appendix C: Camera Mount Details

Trailer structure and mount
Case selection
Case mount to trailer
Case door direction
Case dome
Case mount for camera
Case connecting plate